

Dominant mutations in *ORAI1* cause tubular aggregate myopathy with hypocalcemia via constitutive activation of store-operated Ca²⁺ channels

Yukari Endo^{1,2,4}, Satoru Noguchi^{1,2,*}, Yuji Hara^{5,6}, Yukiko K. Hayashi^{1,2,7}, Kazushi Motomura¹, Satoko Miyatake⁸, Nobuyuki Murakami⁹, Satsuki Tanaka¹⁰, Sumimasa Yamashita¹¹, Rika Kizu¹², Masahiro Bamba¹³, Yu-ichi Goto^{1,3}, Naomichi Matsumoto⁸, Ikuya Nonaka² and Ichizo Nishino^{1,2}

¹Department of Clinical Development, Translational Medical Center, National Center of Neurology and Psychiatry, Kodaira, Tokyo 187-8556, Japan, ²Department of Neuromuscular Research and ³Department of Mental Retardation and Birth Defect Research, National Institute of Neuroscience, National Center of Neurology and Psychiatry, Kodaira, Tokyo 187-8502, Japan, ⁴Department of Pediatrics, Kyoto University Graduate School of Medicine, Kyoto 606-8507, Japan, ⁵Department of Synthetic Chemistry and Biological Chemistry, Graduate School of Engineering, Kyoto University, Kyoto 615-8510, Japan, ⁶Tokyo Women's Medical University Institute for Integrated Medical Sciences (TIIMS), Shinjuku, Tokyo 162-8666, Japan, ⁷Department of Neurophysiology, Tokyo Medical University, Tokyo 160-8402, Japan, ⁸Department of Human Genetics, Graduate School of Medicine, Yokohama City University, Yokohama 236-0004, Japan, ⁹Department of Pediatrics, Dokkyo Medical University, Koshigaya Hospital, Koshigaya, Saitama 343-8555, Japan, ¹⁰Department of Diabetes and Endocrinology, Osaka Saiseikai Nakatsu Hospital, Osaka 530-0012, Japan, ¹¹Division of Pediatric Neurology, Kanagawa Children's Medical Center (KCMC), Yokohama 232-8555, Japan, ¹²Division of Pediatrics, Yokosuka Kyosai Hospital, Yokosuka, Kanagawa 238-8558, Japan and ¹³Division of Pediatrics, Kawasaki Municipal Hospital, Kawasaki, Kanagawa 210-0013, Japan

Received June 28, 2014; Revised August 26, 2014; Accepted September 10, 2014

The store-operated Ca²⁺ release-activated Ca²⁺ (CRAC) channel is activated by diminished luminal Ca²⁺ levels in the endoplasmic reticulum and sarcoplasmic reticulum (SR), and constitutes one of the major Ca²⁺ entry pathways in various tissues. Tubular aggregates (TAs) are abnormal structures in the skeletal muscle, and although their mechanism of formation has not been clarified, altered Ca²⁺ homeostasis related to a disordered SR is suggested to be one of the main contributing factors. TA myopathy is a hereditary muscle disorder that is pathologically characterized by the presence of TAs. Recently, dominant mutations in the *STIM1* gene, encoding a Ca²⁺ sensor that controls CRAC channels, have been identified to cause tubular aggregate myopathy (TAM). Here, we identified heterozygous missense mutations in the *ORAI1* gene, encoding the CRAC channel itself, in three families affected by dominantly inherited TAM with hypocalcemia. Skeletal myotubes from an affected individual and HEK293 cells expressing mutated *ORAI1* proteins displayed spontaneous extracellular Ca²⁺ entry into cells without diminishment of luminal Ca²⁺ or the association with *STIM1*. Our results indicate that *STIM1*-independent activation of CRAC channels induced by dominant mutations in *ORAI1* cause altered Ca²⁺ homeostasis, resulting in TAM with hypocalcemia.

*To whom correspondence should be addressed at: Department of Neuromuscular Research, National Institute of Neuroscience, National Center of Neurology and Psychiatry, 4-1-1, Ogawahigashi-cho, Kodaira, Tokyo 187-8502, Japan. Tel: +81 423461712; Fax: +81 423461742. Email: noguchi@ncnp.go.jp

INTRODUCTION

Calcium (Ca^{2+}) signals are crucial for controlling a broad range of cellular functions, including secretion, excitation, contraction, motility, metabolism, transcription, growth, cell division and apoptosis (1). In the striated muscle, the sarcoplasmic reticulum (SR) is a primary Ca^{2+} -storage organelle, and Ca^{2+} released from the SR directly activates the contraction of myofibrils via excitation–contraction coupling regulation (2). Depletion of Ca^{2+} in the SR activates a store-operated Ca^{2+} entry (SOCE) pathway that is used to replenish intracellular calcium stores (3,4). In non-excitabile cells and the skeletal muscle, SOCE is coordinated by stromal-interacting molecule 1 (STIM1), an endoplasmic reticulum (ER)/SR Ca^{2+} sensor, and ORAI1, a plasma membranous calcium release-activated Ca^{2+} (CRAC) channel, following Ca^{2+} ion release from intracellular stores (5–8). Specifically, when the ER/SR Ca^{2+} store is depleted, oligomerization and translocation of STIM1 to adjacent ER/SR-plasma membrane junctions are induced (9). Within these junctions, oligomeric STIM1 interacts with and activates ORAI1 (10–12).

Recessive mutations in *ORAI1* are known to cause severe combined immunodeficiency (SCID, MIM 612782), which is characterized by a severe defect in T-cell activation accompanied by muscle hypotonia (13,14). In this disease, mutated ORAI1 leads to its deficiency in the plasma membrane resulting in loss of function of SOCE. Homozygous nonsense mutations in *STIM1* also cause primary immunodeficiency (15) (MIM612783). Recently, dominant missense mutations in *STIM1* were revealed to cause tubular aggregate myopathy (TAM) (16). TAM is a rare form of myopathy that can show either autosomal-dominant or -recessive inheritance (17), and is pathologically characterized by the presence of tubular aggregates (TAs). A gain of function of mutated STIM1 due to disruption of its Ca^{2+} -sensing domain was suggested as the main pathomechanism underlying *STIM1*-related TAM. More recently, Stormorken syndrome, which is characterized by thrombocytopenia, muscle fatigue, asplenia and congenital miosis, was also reported to be caused by a gain-of-function *STIM1* mutation (18,19). Stormorken syndrome displays histological evidence of myopathy with TAs (18). However, the mechanism underlying muscle weakness and TA formation from abnormal Ca^{2+} influx has not been well established.

TAs are abnormal structures in muscle fibers that are morphologically characterized based on light and electron microscopic observations (20,21). TAs appear as accumulations of densely packed tubules, which are suggested to arise from the SR as they contain numerous SR proteins (21,22). Conceivably, the formation of TAs is triggered by some functional consequences due to disruptions in the SR-T-tubule junction, such as altered Ca^{2+} homeostasis (20). Alternatively, TAs are thought to be derived from reshaping of the SR caused by aggregation of misfolded membranous proteins (23). TAs are also observed in certain types of muscle diseases, including periodic paralysis, congenital myasthenic syndromes, alcohol- and drug-induced myopathy and TAM (21,22). However, the precise mechanism of TA formation remains to be clarified.

In this study, we performed whole exome sequencing in three families suffering from genetically undiagnosed TAM and found pathogenic mutations in the *ORAI1*. In addition, we demonstrated STIM1-independent activation of CRAC

channels in myotubes derived from an affected individual, suggesting that this abnormal activation is the basic mechanism of this disease.

RESULTS

Clinical characterization of individuals with TAM

The clinical features of the included families are listed in Table 1 and Supplementary Material, Table S1. The common characteristic symptoms among the families were diffuse muscle weakness, marked and bilateral ankle joint contractures, rigid spine and hypocalcemia. Disease onset ranged from childhood to adolescence. Muscle weakness progressed slowly, and although all of the affected individuals were ambulant, half of them required the use of high-heeled shoes to walk correctly. All affected members in Family A and Family B showed mildly decreased serum Ca^{2+} levels and relatively low intact parathyroid hormone (PTH) levels, which were still within the normal range. In computed tomography imaging of II-3a, III-2a and II-3b, paraspinal, gastrocnemius and soleus muscles were markedly replaced by fat, which might explain ankle joint contractures and rigid spine. Trapezius, latissimus dorsi, gluteus medius, hamstrings and adductor muscles in the thigh showed severe atrophy and fat infiltration (Fig. 1). Affected members in Family A also showed central nervous system involvement as follows: individual II-3a showed calcification in the cerebellum, basal ganglia and cerebral corticomedullary junction; individual III-2a showed mild intellectual disability (IQ: 63, based on the Weschler Intelligence Scale for Children III). None of the included individuals showed characteristic signs of Stormorken syndrome, such as congenital miosis, bleeding diathesis and thrombocytopenia (Supplementary Material, Table S1).

Pathological findings

TAs were found in muscle fibers of four affected individuals (II-3a in Fig. 2; I-2b and II-1c in Supplementary Material, Fig. S1; II-1b, pictures not shown). The TAs appeared as bright red inclusions in muscle fibers following modified Gomori trichrome (mGt) staining (Fig. 2A) and showed high enzymatic activity following NADH-tetrazolium reductase (NADH-TR) staining (Fig. 2B), but were negative for succinate dehydrogenase (SDH) expression (Fig. 2C), reflecting characteristics of the SR but not the mitochondria. Under electron microscopy, the TAs appeared as aggregates composed of numerous straight tubules aligned in parallel in a longitudinal dimension and were arranged in a honeycomb-like structure in the transverse dimension (Fig. 2D). At higher magnification, each tubule showed double-walled membranes (Fig. 2E and F). All these findings were compatible with previously reported features of TAs (20). In addition to TAs, all biopsy samples demonstrated chronic dystrophic changes based on the presence of regenerating fibers, increased internal nuclei, fiber size variation in both type 1 and type 2 fibers and endomysial fibrosis. Type 1 fiber predominance was also observed (Table 2).

The *ORAI1* gene is mutated in TAM-affected individuals

In order to identify the genetic cause of dominantly inherited TAM, we performed whole exome sequencing on two affected

Table 1. Clinical characterization of TAM families

| | Family A II-3 | III-2 | Family B I-2 | II-1 | II-3 | Family C II-1 |
|--|---|-------------------------|--------------------|--------------------|--------------------|--------------------|
| Sex | Female | Male | Female | Female | Male | Male |
| Mutation | c.292G>A | c.292G>A | c.292G>A | c.292G>A | c.292G>A | c.412C>T |
| Predicted protein impact | p.Gly98Ser | p.Gly98Ser | p.Gly98Ser | p.Gly98Ser | p.Gly98Ser | p.Leu138Phe |
| Muscle disorders | | | | | | |
| Onset | Childhood | Childhood | NI | Childhood | Childhood | Adolescence |
| Patterns of weakness | Lower limbs proximal; upper limbs proximal | Diffuse | Diffuse | Diffuse | Diffuse | Diffuse |
| Disease course | Slowly progressive | Slowly progressive | Slowly progressive | Slowly progressive | Slowly progressive | Slowly progressive |
| Serum CK (IU/L) (normal range) | 65 (45–170) | 1300 (61–255) | 300 (–200) | 960 (–200) | 684 (–200) | 213 (37–142) |
| Joint contractures | | | | | | |
| Onset | Childhood | Childhood | NI | Childhood | Childhood | Adolescence |
| Ankle | Bilateral, severe | Bilateral, severe | Bilateral, severe | Bilateral, severe | Bilateral, severe | NI |
| Surgical treatment | NP | NP | 13 years old | 10 years old | 11 years old | NP |
| Rigid spine | + | + | + | + | + | + |
| Hypocalcemia | | | | | | |
| Onset | Childhood | Childhood | NI | Childhood | Neonatal | NI |
| Serum calcium (mg/dl) (normal range) | 7.7 (8.8–10.2) | 8.5 (8.8–10.2) | 8.1 (9.0–10.2) | 7.7 (9.0–10.2) | 7.8 (9.0–10.2) | NI |
| Serum intact PTH (pg/ml) (normal range) | 9 (10–65) | NI (NI) | 26 (10–65) | 22 (10–65) | 19 (10–65) | NI |
| Treatment | + | + | NI | NI | + | – |
| Other symptoms | Diabetes, calcification in the brain | Intellectual disability | – | – | – | – |

NI, no information; NP, not performed; CK, creatinine kinase.

(II-3a and III-2a) and two non-affected members (I-2a and III-2a) of Family A and in all five members of Family B (I-1b, I-2b, II-1b, II-2b and II-3b) (Fig. 3A and Supplementary Material, Table S2). In total, 41 variants from Family A and 34 variants from Family B were extracted based on the assumption of autosomal-dominant inheritance and with reference to the dbSNP135, the 1000 Genomes Project database, the National Heart, Lung, and Blood Institute (NHLBI) Exome Variant Server and Human Genetic Variation Database (HGVD) for Japanese genetic variants (Supplementary Material, Table S3). Among all extracted variants, we identified only one common variant, a heterozygous c.292G>A mutation in *ORAI1* (RefSeq accession number NM_032790.3) in both families (Table 1 and Fig. 3A and Supplementary Material, Tables S4 and S5). This mutation was confirmed by Sanger sequencing in all affected members and was absent in the unaffected members (Supplementary Material, Fig. S2). We also found an additional heterozygous missense mutation, c.412C>T in *ORAI1*, in the third TAM family by Sanger sequencing (Fig. 3A and Supplementary Material, Fig. S2). The mutation was not listed in dbSNP137, 1000 Genomes or HGVD. Both mutations were predicted to result in amino acid changes in the ORAI1 protein: p.Gly98Ser in the transmembrane (TM) 1 domain and p.Leu138Phe in the TM2 domain (Fig. 3B). The amino acid residues Gly at 98 and Leu at 138 show high evolutionary conservation (Fig. 3C). The impact of these variations was also predicted to be damaging based on *in silico* analysis with SIFT and PolyPhen-2 (data not shown). The crystal structure of *Drosophila* Orail determined by Hou *et al.* (24) and reported in the Molecular Modeling Database (MMDB ID: 105660) (Fig. 3D) shows that Gly98 is localized to face to the

pore of the CRAC channel (white) and Leu138 is in the interface between TM1 and 2 (yellow).

Localization and expression of ORAI1 in the skeletal muscles from TAM

To analyze the localization of ORAI1 in the skeletal muscles of TAM, we investigated skeletal muscle cryosections from an individual with TAM (II-3a, II-1c) using immunohistochemistry (Fig. 4). SERCA1, an SR protein, was strongly labeled in the aggregates, as previously reported (20,21). ORAI1 and STIM1 co-localized with SERCA1 in the aggregates. Moreover, dihydropyridine receptor (DHPR), which is present in T-tubules, was also involved in the aggregates and co-localized with ORAI1, as expected (21) (Fig. 4).

On western blotting, the expression levels of ORAI1, STIM1, SERCA1 and SERCA2 in the skeletal muscles from an affected individual (II-1c) were similar to that of the skeletal muscles from unaffected individuals (Supplementary Material, Fig. S3).

TAM cells showed constitutive extracellular Ca²⁺ influx via the CRAC channel without depletion of SR Ca²⁺ stores

To explore whether the identified mutations are pathogenic, we monitored Ca²⁺ entry into myotubes prepared from muscle cells of an affected individual with the c.292G>A (p.Gly98Ser) mutation. Intracellular Ca²⁺ concentration ([Ca²⁺]_i) was monitored using Fura-2 as a Ca²⁺ indicator and was recorded by using fluorescence ratiometry with excitation at 340 and 380 nm. The experiments revealed a significantly higher [Ca²⁺]_i level in TAM myotubes than in control cells [normal human skeletal

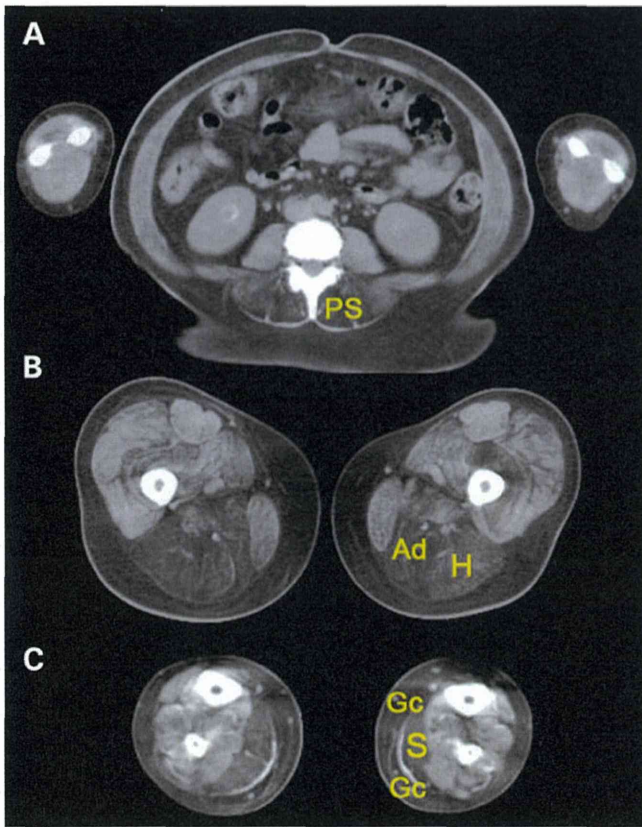


Figure 1. Computed tomographic imaging of TAM. Paraspinal (PS), hamstrings (H), adductor muscles in the thigh (Ad), soleus (S) and gastrocnemius (Gc) muscles of affected individual II-3a were markedly replaced by fat.

muscle cells (SKMCs)] when the extracellular Ca^{2+} concentration was 2 mM, which was assumed to match that of the *in vivo* environment, and 20 mM (Fig. 5A and B). Upon application of a CRAC channel inhibitor, 50 μM 2-aminoethoxydiphenyl borate [2-APB (25)] or 10 μM 3,5-bistrifluoromethyl pyrazole derivative (BTP2) (26), the $[\text{Ca}^{2+}]_i$ levels in TAM myotubes were not elevated (Fig. 5A). Another inhibitor, 1-[2-(4-methoxyphenyl)-2-[3-(4-methoxyphenyl) ethyl]-1H-imidazole hydrochloride (SKF-96365), was also effective although the response was slower. These results indicated that the higher Ca^{2+} influx in TAM myotubes occurred via CRAC channels. In addition, an Mn^{2+} quenching assay of intracellular Fura-2 fluorescence was performed (Fig. 5C). Mn^{2+} is known to enter cells via CRAC channels and shows very high affinity to Fura-2. The extracellular Mn^{2+} influx causes quenching of intracellular Fura-2 fluorescence. TAM myotubes showed an Mn^{2+} quenching that was distinct from that of normal myotubes, implicating the activation of CRAC channels. We also examined thapsigargin (TG) treatment to TAM myotubes to induce Ca^{2+} depletion in the SR. TG induced extracellular Ca^{2+} influx in normal myotubes in a dose-dependent manner in extracellular 2 mM Ca^{2+} medium. On the other hand, similar extracellular Ca^{2+} influx levels were observed in TAM myotubes with and without TG treatment (Fig. 5D). Thus, TAM cells showed constitutive Ca^{2+} influx to the cytosol via the CRAC channel without depletion of the SR Ca^{2+} store. It should be noted that slightly higher $[\text{Ca}^{2+}]_i$ elevation was observed with higher concentrations of

TG treatment (Fig. 5D), indicating that the store-operated Ca^{2+} influx-inducing system may still function in TAM myotubes.

Gly98Ser and Leu138Phe mutations in ORAI1 caused spontaneous activation of the CRAC channel

We also tested the impact of the c.292G>A (Gly98Ser) and c.412C>T (Leu138Phe) mutations in *ORAI1* on induction of spontaneous Ca^{2+} influx. $[\text{Ca}^{2+}]_i$ was measured at 24–36 h after transfection to HEK293 cells of mutated and wild-type *ORAI1* cDNAs. The transfected green fluorescent protein (GFP)-tagged *ORAI1* and Myc-tagged *ORAI1* localized on the plasma membranes, and the mutated *ORAI1* also localized to the cell surface membrane (Fig. 6A). Western blotting of expressed *ORAI1* protein showed multiple bands at 25–50 kDa, indicating the presence of different glycosylated forms, similar to previous reports (27,28) (Fig. 6B). Although glycosylated forms of Gly98Ser-mutated *ORAI1* were slightly decreased, there were no differences in band patterns observed among Gly98Ser-mutated, Leu138Phe-mutated and wild-type (WT) *ORAI1* after PNGase F treatment.

The Gly98Ser and Leu138Phe *ORAI1* mutants caused a dramatic elevation of $[\text{Ca}^{2+}]_i$ following application of 2 mM Ca^{2+} in the medium when compared with the WT protein (2 mM Ca^{2+} in Fig. 6C). Cells transfected with the Gly98Ser or Leu138Phe mutants exhibited high levels of $[\text{Ca}^{2+}]_i$ even under conditions of extracellular Ca^{2+} depletion (0 mM Ca^{2+} region in Fig. 6C). In addition, the Mn^{2+} quenching assay revealed that the cells transfected with Gly98Ser or Leu138Phe mutants showed distinct Mn^{2+} quenching rates from those transfected with the WT protein (Fig. 6D). It should be noted that the spontaneous Ca^{2+} and Mn^{2+} influx observed in the mutated *ORAI1*-expressing cells did not require co-expression of STIM1 or TG-induced Ca^{2+} store depletion in the ER. Moreover, the elevated resting $[\text{Ca}^{2+}]_i$ induced by both *ORAI1* mutants was reduced by application of 2-APB (Supplementary Material, Fig. S4), which indicated the specific activation of CRAC channels. These results clearly demonstrate that both the c.292G>A (Gly98Ser) and c.412C>T (Leu138Phe) mutations in *ORAI1* cause constitutive CRAC channel activation in a STIM1-independent manner.

DISCUSSION

Based on the inheritance mode in the affected families and the functional analyses of mutated *ORAI1* proteins, we concluded that the constitutive activation of CRAC channels by dominant mutations in *ORAI1* caused TAM in the three families. In support of this notion, dominant mutations in *STIM1* have been reported to cause TAM by constitutive activation of SOCE (16). In that report, the mutated *STIM1* spontaneously clustered and translocated to the plasma membrane independently of Ca^{2+} stores in the SR, and consequently led to activation of the CRAC channel, resulting in higher cytosolic Ca^{2+} levels. More recently, Nesin *et al.* (18) reported that activating mutations in *STIM1* and *ORAI1* caused overlapping syndromes of TAM and congenital myosis. Interestingly, the authors suggested that a dominant mutation in *ORAI1* caused prolonged activation

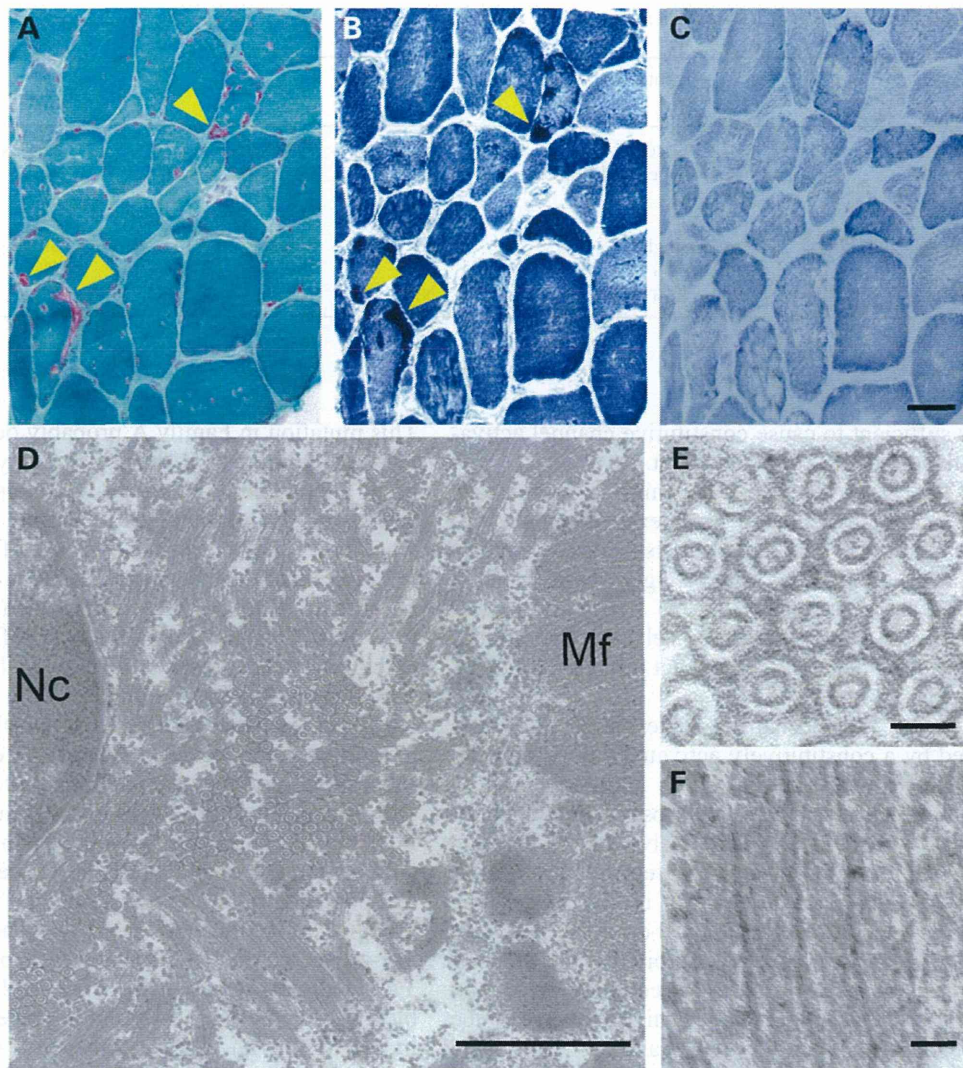


Figure 2. Histology and electron microscopy of a muscle biopsy sample from affected individual II-3a. Histological analysis of transverse sections revealed aggregations with mGt (A) and NADH-TR (B) but not SDH (C) staining. Ultrastructural analysis demonstrated prominent tubular aggregation with double-walled membranes in transversal (D and E) and longitudinal (F) sections. Nc, nucleus; Mf, myofibrils. Arrows, tubular aggregates (TAs). Scale bars, 50 μm (C); 1 μm (D); 100 nm (E); 50 nm (F).

of CRAC channels that required association with STIM1. On the other hand, in the present study, we showed that the two mutations in *ORAI1* directly caused constitutive opening of the channel, resulting in higher cytosolic Ca^{2+} influx independent of either Ca^{2+} stores in the SR or STIM1 activation.

ORAI1 is a tetra-spanning TM protein in the plasma membrane (Fig. 3C) (8), and acts as a pore subunit of the CRAC channel (29). The CRAC channel consists of a hexamer of ORAI1 proteins, and the TM helices (TM1–4) of each monomer are arranged in three concentric rings. Six TM1 helices make up an inner ring of helices and line the ion pore, while the TM2 and TM3 helices constitute a middle ring that surrounds the TM1 helices (24) (Fig. 3D). The mutation c.292G>A (Gly98Ser) was identified in the TM1 domain directly beside the pore (white residues in Fig. 3D). The other mutation, p.412C>T (Leu138Phe), was identified in the TM2 domain directly facing TM1 (yellow residues in Fig. 3D).

Many studies have elucidated the roles of amino acid residues in TM1 in channel activity as well as in the ion selectivity of SOCE channels (8,29–33). In particular, Arg91 is mutated in SCID (13) and is thought to act as both a barrier as well as a provider of electrostatic stabilization to the elongated pore that is controlled via interaction with STIM1, and Glu106 determines ion selectivity (8) (Fig. 3C). Similarly, the importance of Gly98 for channel activity has also been suggested based on *in vitro* experiments (31). Interestingly, Gly98 has been predicted to be located exactly two α -helical turns from both the Arg91 and Glu106 sites (Fig. 3C). Ala replacement at Gly98 results in failure of channel activity, whereas Asp or Pro replacement at this position results in a negative charge or hydrophilic properties, which in turn cause constitutive channel opening as well as reduced ion selectivity in a STIM1-independent manner (31,33). Our experiments revealed that a Ser replacement of Gly at position 98 may also confer the protein with a hydrophilic

Table 2. Histological characterization of TAM families

| | Family A II-3 | Family B I-2 | II-1 | II-3 | Family C II-1 |
|---|----------------------|-----------------|----------------------|--------------|-------------------------|
| Age at muscle biopsy | 42 years | NI | 10 years | 5 years | 42 years |
| Tubular aggregates | Type I and II fibers | + | Type I and II fibers | – | Type I and II fibers |
| Fiber size variation | + | NI | + | + | + |
| Regenerating fibers | + | NI | + | – | + |
| Increased internal nuclei (% of fibers) | Single 14% | NI | Single 15% | Single 5% | Single, multiple 20% |
| Type I fiber predominance (% of fibers) | 70% | NI | 71% | 93% | 73% |

NI, no information.

property that is sufficient to cause constitutive channel activation, similar to the effect of Pro replacement.

In contrast to TM1, the roles of specific amino acid residues in TM2 have not been well investigated. In our experiment, the mutation c.412C>T (p.Leu138Phe) in TM2 also caused constitutive SOCE channel activation. Interestingly, basal $[Ca^{2+}]_i$ levels in Leu138Phe-expressing HEK293 cells were lower than those were in Gly98Ser-expressing cells. Further studies are necessary to fully understand the impact of these mutations on CRAC channels.

Of particular note, the mechanism underlying the muscle weakness caused by a constitutively activated CRAC channel might be associated with altered Ca^{2+} homeostasis in a manner different from that derived from its loss of function. Individuals affected with SCID owing to recessive loss-of-function mutations in *ORAI1* or *STIM1* were reported to show muscle hypotonia (13–15) and decreased Ca^{2+} influx. Transgenic mice with muscle-specific expression of dominant-negative *Orai1* have also been reported and exhibited reduced body weight, muscle mass and fiber cross-sectional area, and increased susceptibility to fatigue, which might have been due to SR Ca^{2+} depletion (34). On the other hand, *ORAI1*-related TAM is caused by elevation of $[Ca^{2+}]_i$ levels in the skeletal muscle cells, similar to *STIM1*-related TAM. Therefore, preventing excessive extracellular Ca^{2+} influx is a potential therapeutic strategy for TAM.

The mechanism of TA formation in the skeletal muscle has remained elusive thus far. However, our results support the hypothesis that TA formation is related to disordered Ca^{2+} homeostasis. Recent efforts on the identification of causative genes in TA-presenting muscle diseases also provide a clue into this mechanism. Recessive mutations in *GFPT1* and *DPAGT1*, which are both involved in protein N-glycosylation, have been shown to be causative factors of myasthenic syndrome with TAs (35,36). Furthermore, the functional importance of N-glycosyl modification of *STIM1* was recently reported (27). A mutation at the N-glycosylation site in *STIM1* results in a strong gain of function by increasing the number of active *Orai1* channels, indicating the significance of N-glycosylation for the function of *STIM1*. Thus, activation of CRAC channels may result in the formation of TAs in skeletal muscles, although further analyses of CRAC channel activation in skeletal muscles of *GFPT1*- and *DPAGT1*-mutated individuals are required to confirm this hypothesis.

The finding of c.292G>A (p.Gly98Ser) *ORAI1* mutation in two unrelated families would not be due to a founder effect.

This mutation in Family A probably occurred *de novo* in II-3a because individual I-1a did not show any symptoms of myopathy in his lifetime and individual I-2a does not have the mutation. Regarding to the mutation in Family B, we could not judge whether it is *de novo* or not, because of limited information.

The clinical and histological features of *ORAI1*-mutated TAM are similar to those of TAM caused by *STIM1* mutations, regarding onset of the disease, progression of weakness, involvement of contractures, presence of TAs in both type I and type II fibers, fiber size variation and type I fiber predominance. However, the patterns of affected muscles are slightly different: individuals with *ORAI1*-mutated TAM exhibit diffuse weakness in all limbs, and the characteristic patterns in the selectivity of atrophy, whereas those with *STIM1*-mutated TAM show proximal muscle weakness only in the lower limbs (16). Severe ankle contractures and a rigid spine were common characteristics observed in the families included in the present study, although *STIM1*-mutated TAM was not likely. Furthermore, eye-movement defects, which were reported in *STIM1*-mutated TAM individuals studied by Böhm *et al.* (16), congenital miosis, bleeding diathesis and thrombocytopenia are not detected in individuals with *ORAI1*-mutated TAM. This discrepancy could be explained by differences in the expression patterns of *STIM1*, *ORAI1* and their homologues (*ORAI2*, *ORAI3* and *STIM2*).

Although *ORAI1* transcripts are expressed in multiple tissues, including the skeletal muscle, in humans and mice (28,37), it is not clear why other organs were saved. *Orai1* expression is low in the brain (28); therefore, the intellectual disability observed in individual III-2a in the present study might be unrelated to the *ORAI1* mutation. The calcification in the brain of individual II-3a could be attributed to long-term hypocalcemia.

Another characteristic clinical feature of *ORAI1*-mutated TAM is hypocalcemia. Serum Ca^{2+} levels are controlled mainly through the action of PTH and 1,25(OH)₂D₃ (38). These hormones increase the serum Ca^{2+} level through their actions on the bone, kidney and intestine; impaired activity of either hormone leads to hypocalcemia. In this study, the five individuals analyzed showed mildly decreased serum Ca^{2+} levels and rather low PTH levels, which were nonetheless within the normal range. PTH is secreted by parathyroid cells and the secretion volume is controlled by the extracellular Ca^{2+} intensity. In *ORAI1*-mutated TAM individuals, PTH levels are improperly low in spite of the presence of hypocalcemia. This condition is classified as PTH-insufficient hypoparathyroidism on the basis of the criteria for the differential diagnosis of hypocalcemia

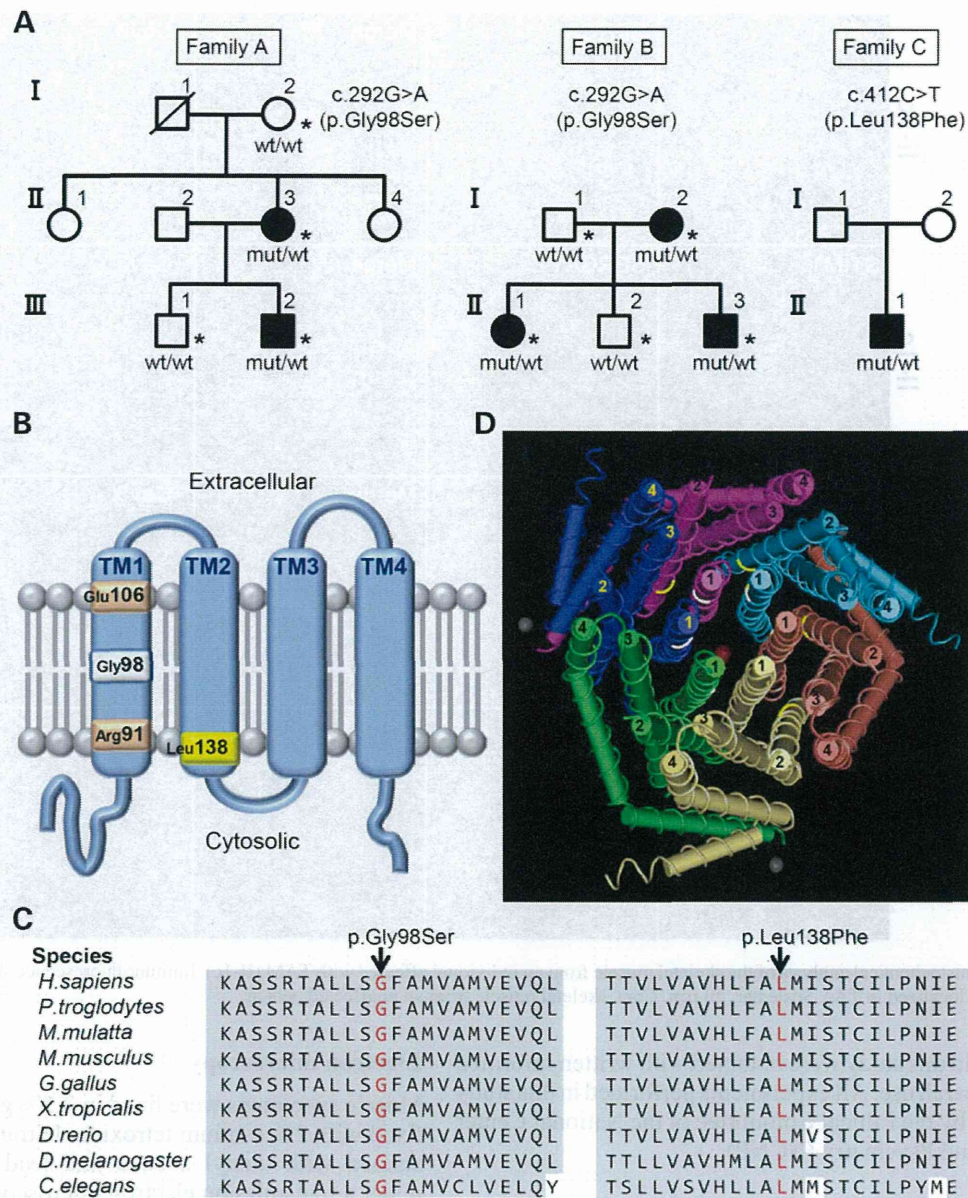


Figure 3. Genetic analysis of autosomal-dominant TAM and modeling the effects of mutations in *ORAI1*. (A) Pedigrees indicated dominant inheritance of TAM, and sequence analysis confirmed the segregation of the heterozygous mutations with the disease. *Individuals who were analyzed by exome sequencing. *ORAI1* genotypes are shown below the individuals in the pedigrees. (B) Schematic depiction of a single *ORAI1* subunit. Upper side, extracellular; lower side, cytosolic. Gly98Ser and Leu138Phe are highlighted in white and yellow, respectively. Arg91 and Glu106, critical amino acids for channel function, are shown in orange. (C) Amino acid sequence conservation of *ORAI1*. The affected amino acids (red) have been highly conserved during evolution. (D) Crystal structure of the *Drosophila melanogaster* SOCE channel. The crystal structure was obtained from the Molecular Modeling Database (MMDB ID: 105660). This structure shows that the channel is formed from a hexamer of *ORAI* subunits. Each subunit is represented in a different color. The ion pore is located at the center of the channel (red circle), and the transmembrane helices are arranged in three concentric rings. Six TM1 helices (1) make up an inner ring of helices and line the ion pore. The TM2 (2) and TM3 (3) helices constitute a middle ring that surrounds the transmembrane portion of the TM1 helices and separates them from TM4 helices (4), which are arranged in an outer ring. The position of Gly98 in TM1 is highlighted in white, and that of Leu138 in TM2 is highlighted in yellow.

(39). Although the precise pathomechanisms are not known, *ORAI1*-mutated TAM might cause decreased PTH secretion.

In summary, we identified heterozygous missense mutations in *ORAI1* that cause TAM with hypocalcemia via constitutive activation of CRAC channels. Our results, together with those of previous reports (16,19), will contribute to establishing a new disease entity whose pathomechanism is associated with intracellular Ca^{2+} elevation to induce muscle weakness and TA formation in the skeletal muscles. The detailed pathomechanism linking

intracellular Ca^{2+} elevation to muscle weakness and TA formation in the skeletal muscles should be clarified.

MATERIALS AND METHODS

Materials

Three unrelated Japanese families affected by TAM were selected based on pathological examinations. All clinical

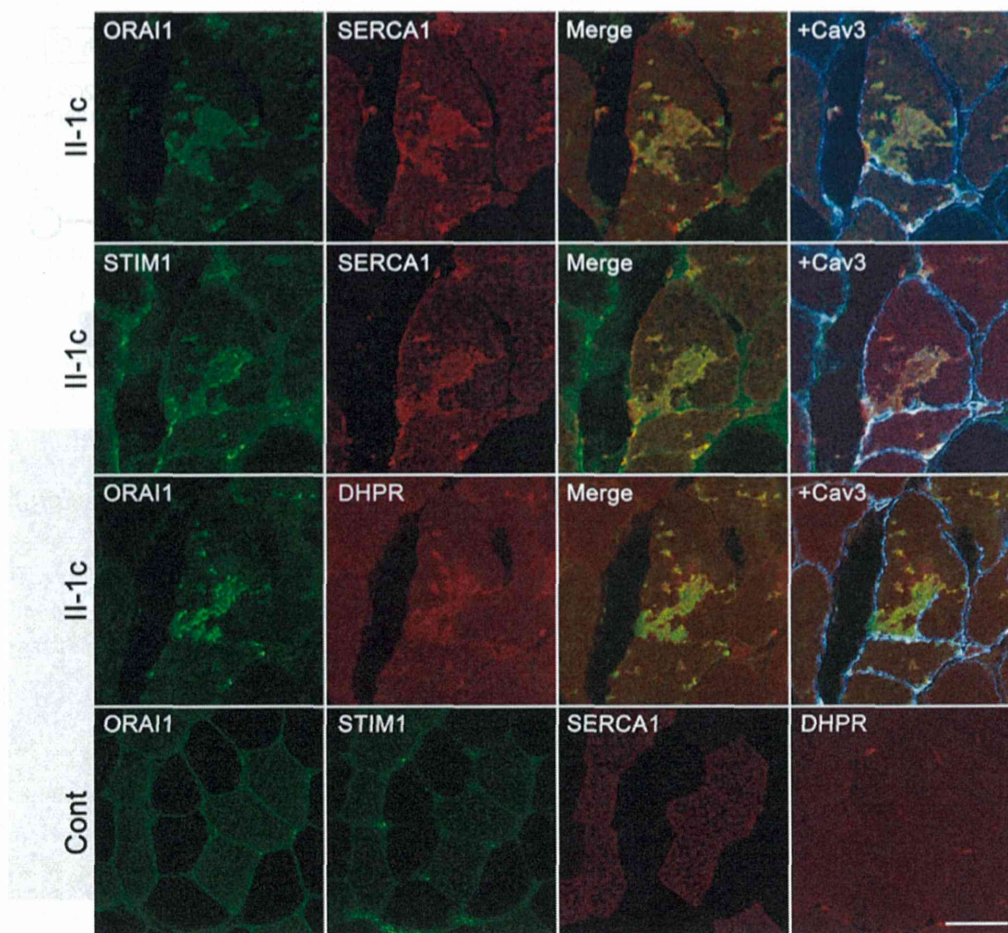


Figure 4. Immunohistochemical analysis of the skeletal muscle from an individual affected with TAM (II-1c). Immunofluorescence showed that SERCA1, ORAI1, STIM1 and DHPR localized in TAs. Scale bar, 50 μ m. Cont, skeletal muscle from an unaffected person.

materials used in this study were obtained with written informed consent for research use. All experiments performed in this study were approved by the Ethical Committee of the National Center of Neurology and Psychiatry (NCNP).

Histological analyses

Muscle samples were taken from the biceps brachii. Muscles were frozen in liquid nitrogen-cooled isopentane and stored at -80°C . Serial frozen sections (10 μ m thick) were histochemically stained with mGt, NADH-TR or SDH. Immunohistochemistry was performed using 8 μ m thick serial frozen sections according to the standard protocols (40). The primary antibodies used were as follows: anti-Orai1 (O8264, 1:200 dilution; Sigma-Aldrich), anti-STIM1 (H-180, 1:50; Santa Cruz Biotechnology), anti-SERCA1 (VE121G9, 1:200; Abcam), anti-RYR1 (XA7B6, 1:200; Developmental Studies Hybridoma Bank) and anti-DHPR (IIID5E1, 1:100; Developmental Studies Hybridoma Bank). Anti-caveolin antibody (N-18, 1:100; Santa Cruz Biotechnology) was also used for labeling the sarcolemma (plasma membrane of the muscle fiber). After incubation with primary antibodies, the sections were incubated with appropriate Alexa Fluor 488-, 568- and 647-conjugated secondary antibodies (1:600; Invitrogen). The sections were observed under an LSM710 confocal laser microscope (Carl Zeiss).

Electron microscopy

Muscle specimens were fixed in 2.5% glutaraldehyde and post-fixed with 2% osmium tetroxide. Ultrathin sections of muscles stained with uranyl acetate and lead citrate were observed under a transmission electron microscope (FEI; Hillsboro, OR, USA).

Exome sequencing

Genomic DNA was isolated from muscle specimens or peripheral blood lymphocytes using standard techniques. Exome sequencing was carried out in subjects I-2a, II-3a, III-1a and III-2a from Family A, and in subjects I-1b, I-2b, II-1b, II-2b and II-3b from Family B. Exons of genomic DNA samples were captured and sequenced using Agilent in-solution enrichment methodology and the Illumina HiSeq1000 sequencer. Briefly, 3 μ g of each genomic DNA sample was fragmented to 150–200 bp by sonication. Paired-end fragment libraries were prepared by using a kit from Agilent Technologies. Purified libraries (750 ng) were hybridized to the SureSelect oligonucleotide probe capture library for 24 h (Sure Select Human All Exon kit V4, 50 Mb; Agilent). The captured DNA sample was then sequenced on an Illumina HiSeq1000 as paired-end 100-base reads. Image analysis and base calling were performed using

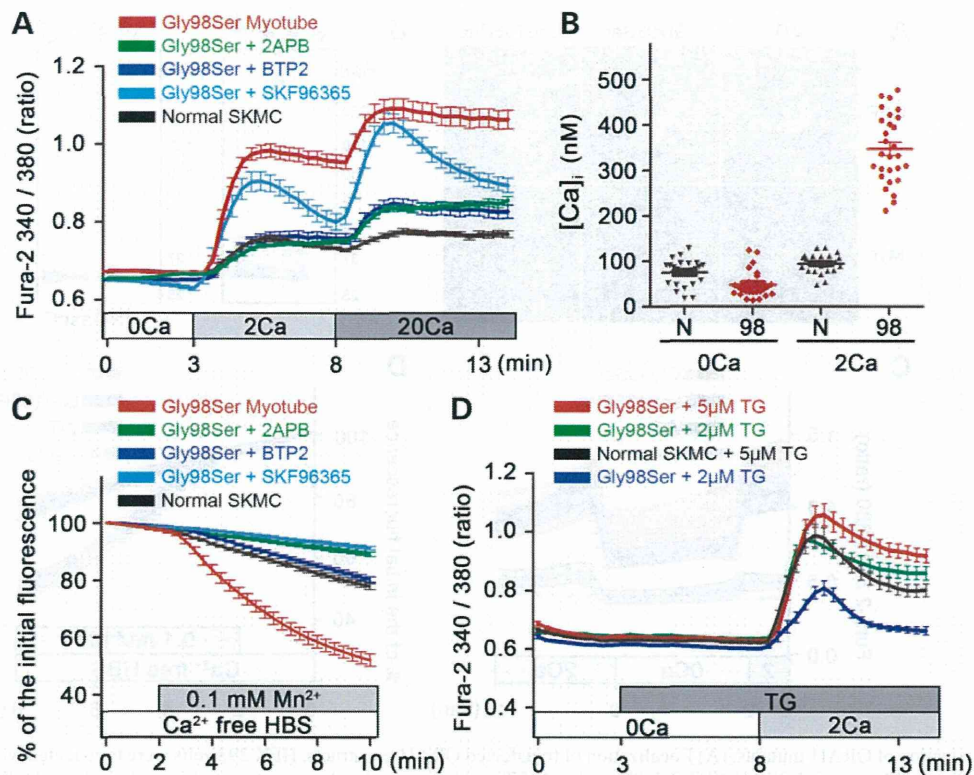


Figure 5. Cytosolic Ca^{2+} measurement and Mn^{2+} quenching assay of myotubes from an individual affected with TAM. (A) Cytosolic Ca^{2+} was measured with Fura-2 in myotubes from affected individual II-3b (red: Gly98Ser myotube, $n = 29$ cells) and normal human skeletal muscle (black: normal SKMC, $n = 26$ cells), using single-cell Ca^{2+} imaging. First, cells were placed in an extracellular solution containing 0 mM Ca^{2+} (0Ca). After 3 min, the extracellular solution was changed to 2 mM Ca^{2+} (2Ca), and then to 20 mM Ca^{2+} (20Ca) at 8 min. Myotubes from affected individual were experimentally treated with $50 \mu\text{M}$ 2-APB (green: Gly98Ser + 2APB, $n = 17$ cells), with $10 \mu\text{M}$ BTP-2 (blue: Gly98Ser + BTP2, $n = 17$ cells) or with $20 \mu\text{M}$ SKF96365 (cyan: Gly98Ser + SKF96365, $n = 15$). (B) Resting $[\text{Ca}^{2+}]_i$ in myotubes from TAM. 0Ca, N: normal SKMC98, $n = 26$; 0Ca, 98: Gly98Ser myotube, $n = 25$; 2Ca, N: normal SKMC98, $n = 27$; 2Ca, 98: Gly98Ser myotube, $n = 28$. (C) Fluorescence quenching due to the Mn^{2+} influx was observed in Fura-2-loaded Gly98Ser myotubes (red, $n = 32$ cells) and normal SKMC myotubes (black, $n = 21$ cells), using single-cell Ca^{2+} imaging. Mn^{2+} (0.1 mM) was added to nominally Ca^{2+} -free HBS. Gly98Ser myotubes were treated with $50 \mu\text{M}$ 2-APB (green: Gly98Ser + 2APB, $n = 17$ cells), with $10 \mu\text{M}$ BTP-2 (blue: Gly98Ser + BTP2, $n = 17$ cells) or with $20 \mu\text{M}$ SKF96365 (cyan: Gly98Ser + SKF96365, $n = 39$ cells). (D) Store-operated Ca^{2+} entry in myotubes. Ca^{2+} stores in the SR were depleted by treatment with $2 \mu\text{M}$ TG or $5 \mu\text{M}$ TG. Red, Gly98Ser myotubes with $5 \mu\text{M}$ TG, $n = 20$ cells; green, Gly98Ser myotubes with $2 \mu\text{M}$ TG, $n = 25$ cells; black, normal SKMC myotubes with $5 \mu\text{M}$ TG, $n = 27$ cells; blue, normal SKMC myotubes with $2 \mu\text{M}$ TG, $n = 25$ cells.

the Illumina Real-Time Analysis Pipeline version 1.13, with default parameters.

Bioinformatics analysis

Reads were aligned to hg19 with Burrows-Wheeler Aligner (41). Duplicate reads were removed using Picard for downstream analysis. Local realignments around indels and regions for low base quality scores were performed with the Genome Analysis Toolkit (42) (GATK) for recalibration. Single-nucleotide variants and small indels were identified using GATK UnifiedGenotyper (version 1.6) and filtered according to the Broad Institute's best-practice guidelines. Genetic variation was annotated with the NCNP in-house pipeline (amelief), consisting of gene annotation [using ANNOVAR (43)] and detection of known polymorphisms using dbSNP135, the 1000 Genomes, NHLBI Exome Variant Server (ESP5400) and HGVD for Japanese genetic variants. Candidates of mutations identified in exome sequencing were validated by Sanger sequencing on an ABI Prism 3130 DNA Analyzer (Applied Biosystems). Segregation analysis of within-family variants was carried out using the

primer sets designed to amplify exons corresponding to the sequence under accession NM_032790. PCR conditions and primer sequences for *ORAI1* mutation analysis are available upon request.

Western blotting of the skeletal muscles

Frozen skeletal muscles were sliced and suspended in the buffer containing 10 mM Tris-HCl, 0.6 mM KCl and 1 mM EDTA. After a centrifugation at $1200g$ for 10 min , the supernatant was centrifuged at $20\,000g$ for 90 min . The resulting pellet was solubilized in laemmli's sample buffer. An equal amount of proteins ($10 \mu\text{g}$) were electrophoresed on 4–20% polyacrylamide gradient gel (Bio-Rad). The primary antibodies used were as follows: anti-Orai1 (O8264, 1:1000 dilution; Sigma-Aldrich), anti-STIM1 (H-180, 1:500; Santa Cruz Biotechnology), anti-SERCA1 (VE121G9, 1:1000; Abcam) and anti-caveolin-3 antibody (Clone 26, 1:1000; BD Transduction Laboratories). The blots were coupled with the peroxidase-conjugated secondary antibodies, and developed using the ECL detection kit (Millipore Corporation).

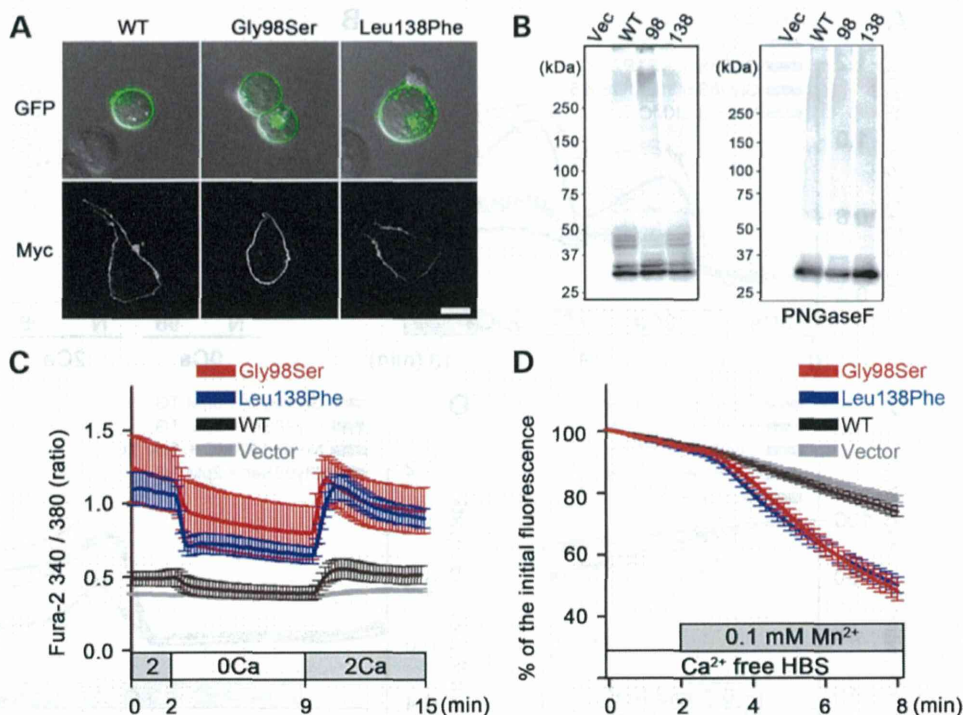


Figure 6. Characterization of ORAI1 mutants. (A) Localization of transfected ORAI1 constructs. HEK 293 cells were transfected with EGFP-tagged ORAI1 (WT, Gly98Ser, Leu138Phe) or Myc-tagged ORAI1 (WT, Gly98Ser, Leu138Phe). Upper panels, phase contrast (white and black) and GFP fluorescence (green). Lower panels, fluorescent micrographs for Myc-ORAI1. (B) Western blot of Myc-tagged ORAI1 proteins expressed in HEK cells (left panel). PNGaseF treatment (right panel). Vec, vector; 98, ORAI1 with Gly98Ser; 138, ORAI1 with Leu138Phe. (C) Cytosolic Ca^{2+} was measured in HEK293 cells expressing WT ORAI1 (black, $n = 35$ cells) and ORAI1 mutants, Gly98Ser (red, $n = 28$ cells) or Leu138Phe (blue, $n = 37$ cells) and vector (gray, $n = 32$ cells). Extracellular solution was first changed to 0 mM Ca^{2+} (0Ca) then to 2 mM Ca^{2+} (2Ca). (D) Mn^{2+} quenching assay. After application of 0.1 mM Mn^{2+} solution, fluorescence quenching of Fura-2 was observed in HEK293 cells expressing WT ORAI1 (black, $n = 34$ cells) and ORAI1 mutants, G98S (red, $n = 42$ cells) or L138F (blue, $n = 43$ cells), and vector (gray, $n = 46$ cells).

Construction of ORAI1 mutants

The construction of WT and mutant human *ORAI1* cDNA in the expression vectors pCMV-Myc and pEGFP-N1 (Clontech) was described previously (44). A Myc tag was fused to the N-terminus of ORAI1, and a EGFP tag was fused to the C-terminus of ORAI1 without its termination codon. All *ORAI1* mutants were generated with the Quick Change Site-Directed Mutagenesis Kit (Stratagene). Information on primer sequences and conditions for cloning and PCR is available upon request.

Transfection of ORAI1 constructs to HEK293 cells

HEK293 cells obtained from the RIKEN Bioresource Center were maintained in Dulbecco's modified Eagle medium (D-MEM; Wako) supplemented with 10% fetal bovine serum (FBS; Life Technologies), 2 mM glutamine, 30 units/ml penicillin and $30 \mu\text{g/ml}$ streptomycin. *ORAI1* constructs were transfected using X-tremeGENE9 (Roche Applied Science). For observation of ORAI1 mutants in cells, EGFP-tagged *ORAI1* constructs were also introduced. For western blots, Myc-tagged *ORAI1* constructs were introduced. For $[\text{Ca}^{2+}]_i$ measurement, Myc-tagged *ORAI1* constructs were co-transfected with the pDsRed-Monomer-C1 vector (Clontech).

Localization of ORAI1 protein in HEK293 cells

Confocal and phase contrast images were taken at 2 days post-transfection on an LSM-710 microscope (Carl Zeiss).

Expression of ORAI1 protein in HEK293 cells

HEK293 cells were harvested at 2 days post-transfection. The cells were lysed with Tris-buffered saline containing 1% Triton X-100 and protease inhibitors (cComplete EDTA-free; Roche). The extracts were boiled in the presence of sodium dodecyl sulfate sample buffer and subjected to western blot analysis. An equal amount of the supernatant fractions ($75 \mu\text{g}$ proteins) was subjected to SDS-PAGE (SuperSep Ace, 5–20% gradient gel, Wako). The protein-transferred membrane was incubated with anti-Myc antibody (9E10, 1:2000; Wako). After incubating with anti-mouse IgG (H+L) secondary antibody conjugated with horseradish peroxidase (GE Healthcare), the expression of ORAI1-Myc was detected using Immunostar Zeta (Wako). To confirm glycosylated patterns of ORAI1, lysate samples ($75 \mu\text{g}$ each) were incubated with PNGase F (Roche; 3 U/sample), for 6 h at 37°C and subjected to SDS-PAGE.

Cell culture for $[\text{Ca}^{2+}]_i$ measurement and Mn^{2+} quenching assay

Skeletal muscle cells of a TAM-affected individual (II-3b) and normal human SKMCs (Clonetics) were seeded onto collagen-coated glass cover slips and cultured in D-MEM/Ham's F-12 medium (1:1) supplemented with 20% FBS (Invitrogen), 100 units/ml penicillin and $100 \mu\text{g/ml}$ streptomycin. After the cells reached confluence, the culture media were switched to differentiation media [D-MEM/Ham's F-12 Medium (1:1)